

## STRUCTURAL, OPTICAL AND DIELECTRIC PERFORMANCE OF MOLYBDENUM TRIOXIDE THIN FILMS SANDWICHED WITH INDIUM SHEETS

M. ABUSAA<sup>a</sup>, A. F. QASRAWI<sup>a,c</sup>, H. K. KMAIL<sup>a</sup>, H. K. KHANFAR<sup>b,\*</sup>

<sup>a</sup>*Department of Physics, Arab American University, Jenin, Palestine*

<sup>b</sup>*Department of Telecommunication Engineering, Arab American University, Jenin, Palestine*

<sup>c</sup>*Faculty of Engineering, Atilim University, 06836 Ankara, Turkey*

In this work, we report the enhancements in the structural, optical and dielectric properties of molybdenum trioxide that are achieved by insertion of 50 and 100 nm thick indium sheets between layers of MoO<sub>3</sub>. The films which are coated onto ultrasonically glass substrates under a vacuum pressure of 10<sup>-5</sup> mbar exhibited metal induced crystallization process upon insertion of indium sheets. Optically, indium sheets tuned the transmittance and reflectance, significantly, increased the absorption coefficient values and formed interbands in the band gap of MoO<sub>3</sub>. The energy band gap decreased with increasing indium sheets thickness. On the other hand, the insertion of indium layers into the structure of MoO<sub>3</sub> is observed to improve the dielectric response of these films to values that nominate them for used in thin film transistor technology. In the same context, the analyses of the optical conductivity which are carried out with the help of Drude-Lorentz approach have shown that the presence of indium sheets can increase the optical conductivity and enhance the plasmon frequency and free charge carrier density of MoO<sub>3</sub>. The plasmon frequency is tuned in the range of 1.68-7.16 GHz making MoO<sub>3</sub> films attractive for plasmonic applications.

(Received September 15, 2020; Accepted November 2, 2020)

*Keywords:* MoO<sub>3</sub>/In/MoO<sub>3</sub>, X-ray, EDS, Dielectric dispersion, Optical conduction

### 1. Introduction

Molybdenum trioxide thin films are accounted as optoelectronic materials which have wide range of applications. MoO<sub>3</sub> is employed in the fabrication of solar cells [1], supercapacitors [2], high- $\kappa$  gate thin film transistors [3], photodiodes [4] and microwave band filters [5]. Recently, high power efficiency solar cells (of about 9.2% ) were fabricated by using multilayers of MoO<sub>3</sub>/Ag/MoO<sub>3</sub> electrodes [1]. The open circuit voltage and short circuit current density of this device reached 0.93 V and 19.59 mA/cm<sup>2</sup>, respectively. In addition, as supercapacitors, the electrochemical analyses on the  $\alpha$ -MoO<sub>3</sub> and  $\alpha$ -MoO<sub>3</sub>/MnO<sub>2</sub> composite materials have shown that these capacitors could exhibit specific capacitance of 76 F/g and 109 F/g, respectively, nominating these two materials as low-cost high-performance supercapacitors [2]. Moreover, MoO<sub>3</sub>/p-Si heterojunction devices which are employed as photodetectors that are tested under near infrared (1100 nm) irradiation level displayed fast rise time of 72.32 ms and fall time of 68.15 ms. Such ultrafast detectors are promising for use in harvesting infrared energy for solar cells and photo-sensing applications [4]. Furthermore, the direct current and impedance spectroscopy measurements on the Yb/MoO<sub>3</sub>/(C, Yb) thin film devices have shown its usability as tunable metal-oxide-semiconductor MOS devices.<sup>5</sup> This device displayed high rectification ratios of 1.26×10<sup>4</sup> at biasing voltage of 0.5 V making them suitable as electronic switches. As microwave low/high pass band filters, it also displayed microwave cutoff frequency and return loss values of 140 GHz and 26 dB at 1.8 GHz, respectively [5].

Modern studies that concern enhancement of the performance of molybdenum oxide has employed the insertion of metal sheets between layers of MoO<sub>3</sub> as an alternative technique [1,6,7] to the traditional doping techniques. For example, the change of the metal in the MoO<sub>3</sub>/metal/MoO<sub>3</sub> structure is reported to successfully tune the transparency of solar cells and

\* Corresponding authors: Hazem.Khanfar@aaup.edu

change their power efficiency, open circuit voltage and short circuit current values [6]. While metal slabs of 20 nm thick of Ag increased the short circuit current density to 3.5 mA/cm<sup>2</sup>, slabs of Au with the same thickness increased the current density to 5.5 mA/cm<sup>2</sup> [6]. On the other hand, energy band gap and optical conductivity parameters engineering was possible for MoO<sub>3</sub>/Li/MoO<sub>3</sub> films by altering the thickness of lithium [7]. Particularly, 20, 50, 100 and 200 nm thick layers of lithium decreased the band gap from 3.05 eV to 1.88, 1.78, 1.1 and 0.47 eV, respectively. The drift mobility of this system increased from 5.86 to 11.7 and 11.4 cm<sup>2</sup>/Vs upon insertion of 20 and 50 nm thick layers of Li, respectively. In another parallel work, molybdenum trioxide was sandwiched with indium slab of thickness of 200 nm to form Au/MoO<sub>3</sub>/In/MoO<sub>3</sub>/C device [8]. Electrical characterization on this films which are coated onto Au thin film substrates revealed novel features presented by negative capacitance effect above indicating the applicability of the Au/MIM/C structures as microwave cavities and parasitic capacitance cancellers in electronic circuits.

In the light of these remarkable enhancements, and as an alternative type of application, we are motivated to study the effect of indium sheets on the performance of MoO<sub>3</sub> films. Namely, the effect of 50 and 100 nm thick indium layers on the structural, compositional, optical and dielectric performance of MoO<sub>3</sub> will be reported. In addition, the effect of indium sheets on the optical conductivity parameters will be explored through the Drude-Lorentz model analysis to investigate the changes in the drift mobility, free carrier density and plasmon frequency of the MoO<sub>3</sub>/In/MoO<sub>3</sub> structure.

## 2. Experimental details

Molybdenum trioxide thin films of thicknesses of 500 nm are prepared by the thermal evaporation technique using VCM-600 thermal evaporator under vacuum pressure of 10<sup>-5</sup> mbar. The source material was high purity (99.99%) MoO<sub>3</sub> powders. The films which were coated onto chemically and ultrasonically cleaned glass substrates were re-coated with indium sheets of thicknesses of 50 and 100 nm using the same system. The produced MoO<sub>3</sub>/In films were kept in the VCM-600 vacuum system until another layer of MoO<sub>3</sub> was recoated to form MoO<sub>3</sub>/In/MoO<sub>3</sub> (MIM) trilayers. The thicknesses of the films were recorded with the help of Inficon –STM-2 quartz crystal monitor which has resolution of 0.03 Å and can carry 3000 reading per second. The structure and composition of the films was explored by Miniflex-600 X-ray diffraction unit and by EDAX type energy dispersive X-ray analyzer, respectively. The optical transmittance and reflectance spectra were recorded with the help of Evolution 300 spectrophotometer. While the X-ray was recorded in the diffraction angle range of 10-70°, the compositional analyses were carried out at accelerating voltage of 11 keV and the optical spectra were recorded in the range of 300-1100 nm. Both of the transmittances and reflectance spectra were recorded at normal incidence.

## 3. Results and discussion

In this work, we targeted engineering the optical and dielectric properties of MoO<sub>3</sub> via insertion of indium sheets of thicknesses of 50 and 100 nm between two stacked layers of MoO<sub>3</sub>. Each MoO<sub>3</sub> layer is of thickness of 500 nm. As one may observe from the inset of Fig. 1, while the MoO<sub>3</sub> ((given the code M) thin films exhibit off-white color, those coated with 50 nm indium show dark green color and when the MoO<sub>3</sub>/In ((given the code MI)) films are re-coated with another layer of MoO<sub>3</sub> to form MoO<sub>3</sub>/In/ MoO<sub>3</sub> (MIM) the sample color converts to purple. The change in the colors of the films indicates attenuation in the optical transmittance and reflectance of the films under study. On the other hand, the X-ray diffraction (XRD) patterns for MM-0, MIM-50 and MIM-100 samples which are shown in Fig. 1 display metal induced crystallization process as a result of indium sheets insertion between layers of molybdenum trioxide.

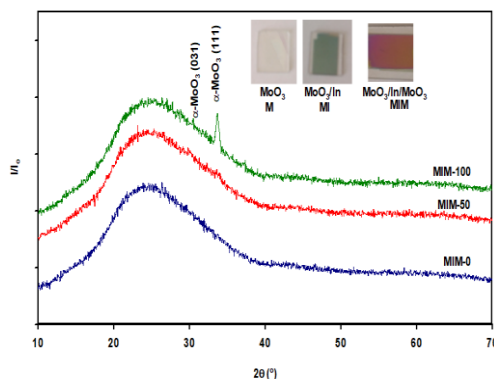


Fig. 1. the X-ray diffraction patterns for the  $\text{MoO}_3/\text{In}/\text{MoO}_3$  films. The inset shows the optical image of the samples.

Particularly, while the two stacked layers of  $\text{MoO}_3$  and those which contain 50 nm thick layers of indium display no sharp XRD patterns reflecting the amorphous nature of structure, the increase in the indium nanosheet thickness from 50 to 100 nm resulted in sharp peaks centered at diffraction angles of  $2\theta = 33.75^\circ$  and another broaden peaks centered at  $2\theta = 30.55^\circ$ . Analysis of the XRD patterns in accordance with the published literature data<sup>5</sup> and PDF cards (35–0609) have shown that these two peaks are assignable to the orthorhombic  $\text{MoO}_3$  which exhibits lattice parameters of  $a = 3.962 \text{ \AA}$ ,  $b = 13.8600 \text{ \AA}$  and  $c = 3.697 \text{ \AA}$ .<sup>5</sup> Particularly, as the observed peak numbers are insufficient to explore the real structure, we have used the PDF cards and published data to pick up the lattice parameters and insert them into a simulating software package “Crystdiff” that can reproduce the X-ray patterns and allow comparisons with experiments. All possible structural phases of  $\text{MoO}_3$  (monoclinic, orthorhombic, tetragonal and hexagonal),  $\text{In}_2\text{O}_3$  and pure indium were tested. The possible reflection planes that coincide with the experiment are shown in the figure. The best correlation between the experiment and simulator which involve no error is related to the orthorhombic phase of  $\text{MoO}_3$ . Similar crystallization process of  $\text{MoO}_3$  with the same nature of structure was observed for films coated onto nontransparent (1.0  $\mu\text{m}$  thick) ytterbium substrates [5]. The crystalline phase which is achieved by the indium sheets is different from that we previously observed by the insertion of lithium sheets [7]. The insertion of 50 nm thick Li sheets induced the formation of both of the monoclinic and hexagonal  $\text{MoO}_3$ . For the currently reported orthorhombic structure the calculated structural parameters presented by crystallite size ( $D$ ), microstrain ( $\epsilon$ ), stacking faults percentage ( $SF\%$ ) and defect density ( $\delta$ ) are found to be 22 nm,  $5.8 \times 10^{-3}$ , 0.32% and  $1.00 \times 10^{10} \text{ lines/cm}^2$ . Although the insertion of Li sheets leads to larger crystallites and less microstrain, the insertion of indium sheets of the same thickness causes less defect density compared to that of  $\text{MoO}_3/\text{Li}/\text{MoO}_3$  films [7] which displayed value of  $6.75 \times 10^{10} \text{ lines/cm}^2$ . Replacement of Li by indium causes reduction in defect density by 85.2%. The less the defect density, the more stable the materials surface [9].

While the ionic radius of Li being 60 pm [7] is very close to that of  $\text{Mo}^{+6}$  (62 pm), the ionic radius of  $\text{In}^{+3}$  being 81 pm [10] is larger than that of  $\text{Mo}^{+6}$  indicating the less probability of substitution of indium in vacant sites of molybdenum. However, since the bond length of In-O being 210 pm [11] is less than that of Mo-O(2) which exhibit value of 225 pm [7], formation of  $\text{In}_2\text{O}_3$  at the ultrathin interface between  $\text{MoO}_3$  and indium sheets is preferable. The inability to observe this phase by the X-ray measurements should be attributed to the thickness of indium layer. Particularly, in our earlier investigation [8] we were able to detect peaks of  $\text{In}_2\text{O}_3$  when we inserted a non-transparent indium sheet of thickness of 200 nm between two layers of  $\text{MoO}_3$ . In the current study with the optically transparent thicknesses of indium being 50 and 100 nm we were not able to detect the phase of  $\text{In}_2\text{O}_3$ . When such bonding take place, defect density reduction is expected. This is just because indium atoms complete the bonding with unbonded oxygen atoms which behave as a trap for positive interstitial ions [12]. Earlier studies on metal induced crystallization processes on Si have shown that the amount of crystallized silicon depends on the quantity of Al.

This mechanism is reported to be actualized through intermixing of Al with Si and the formation of an alloy of high metal concentration at the amorphous/crystalline interfaces [13]. Similar to our samples which contained thin layer of indium (50 nm), the formation of the Si-Al alloy was not assured due to low Al concentration. It is mentioned that the crystallization does not start unless sufficient amount of metal is involved in the volume of the semiconductor.<sup>13</sup> Our energy dispersive X-ray spectroscopy measurements on the studied samples which are illustrated in Fig. 2 have shown that the atomic content of indium in the MIM-50 sample is 3.77 at. % and the atomic content of indium in the MIM-100 samples is 12.46 at.%. In addition, no change in the atomic content of Mo was observed upon indium participation in the structure of the films. These numerical values suggest that the 12.46 at. % of indium is sufficient to induce the crystallization process in  $\text{MoO}_3$  and the content value being 3.77 at.% (MIM-50) is still below the limit needed for initiation of the crystallization process in  $\text{MoO}_3$  films.

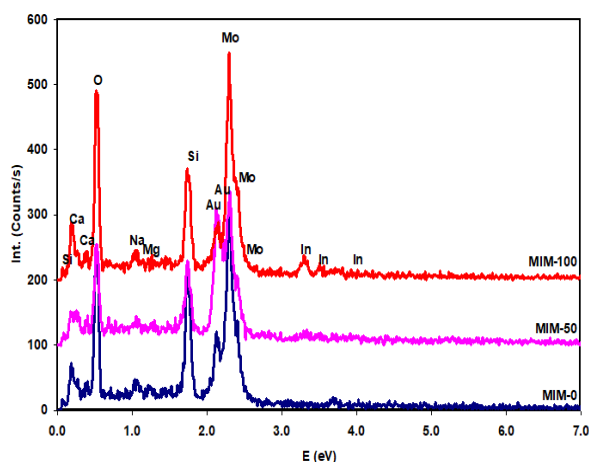


Fig. 2. The energy dispersive X-ray spectroscopy for the  $\text{MoO}_3/\text{In}/\text{MoO}_3$  films.

Fig. 3 (a) and (b) illustrates the transmittance ( $T$ ) and reflectance ( $R$ ) spectra for the two stacked layers of  $\text{MoO}_3$  and tacked layers of  $\text{MoO}_3$  which contain indium sheets in its volume. As seen from Fig. 3 (a), the transmittance spectra of the MIM-0 films exhibit local and absolute maxima of 72.7% and 87.2% at 414 nm and 536 nm, respectively. Insertion of 50 nm thick indium sheets lowered the transmittance by more than 50%. For MIM-50 broaden peaks of value of 14.3% appeared at 390 nm. The absolute maxima for this sample exhibit value of 39.0% at 484 nm. Increasing the thickness of the indium nanosheet to 100 nm, lowered  $T$  values further. For MIM-100, broaden peaks of 6.5% appeared at 376 nm and absolute maxima of value of 16.0% is centered at incident light wavelength of 516 nm. On the other hand, the reflectance spectra which are shown in Fig. 3 (b) displayed three peaks of values of 16.1%, 20.0% and 16.6% centered at 368, 452 and 684 nm, respectively, for MIM-0 samples two peaks of values of 27.7% and 25.6% centered at 394, 586 nm, respectively for MIM-50. Increasing the thickness of the indium layers to 100 nm redshifts these two peaks and increases their values. Namely the two peaks exhibit values of 36.3% and 28.7 % at 422 and 624 nm, respectively.

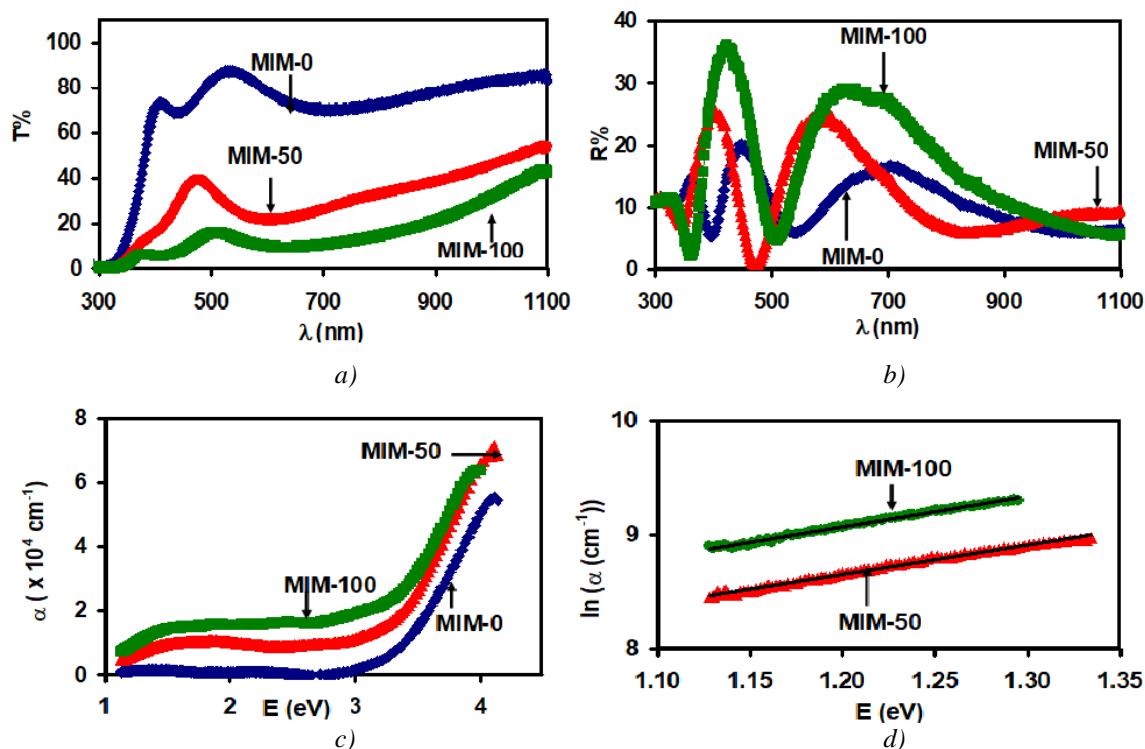


Fig. 3. The optical (a) transmittance, (b) reflectance and (c) absorption coefficient spectra and (d) the  $\ln(\alpha) - E$  variations for  $\text{MoO}_3/\text{In}/\text{MoO}_3$  films.

The absorption coefficient ( $\alpha$ ) spectra which are calculated with the help of the previously reported equations [14] are illustrated in Fig. 3 (c). It is clear from the figure that the insertion of indium sheets increases the value of the absorption coefficient and redshifts the absorption edge. The absorption coefficient in the incident photon energy range of 3.0-1.5 eV exhibits values that do not depend on incident photon energy but increases with increasing indium sheets thicknesses. For example, at 3.0 eV, the absorption coefficient values increases from  $1.92 \times 10^3 \text{ cm}^{-1}$  to  $1.19 \times 10^4 \text{ cm}^{-1}$  and to  $1.93 \times 10^4 \text{ cm}^{-1}$  as the indium nanosheet thickness increases from 0 to 50 and reaches 100 nm, respectively. Significant enhancement in the light absorbability by 6.2 and 10.1 times is, respectively, achieved. It is also noticeable that in the low incident photon energy range (1.4-1.1 eV), the absorption coefficient start decreasing with decreasing incident photon energy. This behavior which was previously observed for pure  $\text{MoO}_3$  coated with CdSe was assigned to the formation of interbands in the energy band gap of the molybdenum trioxide [15]. The width of the interbands ( $E_e$ ) is estimated from the plots of the  $\ln(\alpha) - E$  variations [15] which are illustrated in Fig. 3 (d). The slopes of the solid lines reveal the values of  $E_e$  as 0.39 and 0.37 eV for MIM-50 and MIM-100, samples, respectively. These values of interbands widths are wider than those we determined as 0.20 eV for the  $\text{MoO}_3/\text{CdSe}$  interfaces [15]. Interbands transitions in the ultraviolet range were observed for hetero-nanostructured Ag nanoparticles/ $\text{MoO}_3$  nanobelts composites and was assigned to the transitions in the  $(\text{MoO}_6)^{6-}$  octahedrons by trapping electrons of  $\text{Mo}^{6+}$  to form  $\text{Mo}^{5+}$  [16]. Interbands transitions in the infrared range of light in pure  $\text{MoO}_3$  are not observed. The formation of the interbands and the enhanced light absorbability that is achieved via indium sheets insertion between layers of molybdenum trioxide most probably assigned to the formation of  $\text{In}_2\text{O}_3$  bonds at the ultrathin part of the interface as we mentioned in the X-ray diffraction part. The exchange in the bonding of O(2) in  $\text{MoO}_3$  from Mo-O(2) to In-O owing to the shorter bond length of In-O may lead to the atomic overlapping which forms band tails in the band gap of  $\text{MoO}_3$  [15]. Indium thin films are known to exhibit interbands transitions due to the transition of electrons from bound levels to the empty states of the overlapping conduction 5s, 5p

bands [17]. Since the electronic configuration of indium is  $4d^{10} 5s^2 5p^1$  and that of Mo is  $4d^5 5s^1$ , strong atomic orbital overlapping is expected between the two elements leading to the observed interbands.

The effect of the indium sheets on the optical energy band gap of molybdenum trioxide is explored with the help of Tauc's equation ( $(\alpha E)^{1/2} \propto (E - E_g)$ ) for indirect allowed transitions [5,7,14,15]. The plots of the  $(\alpha E)^{1/2} - E$  variations which are presented in Fig. 4 (a) revealed straight lines that are restricted to exhibit the same residual sums of squares ( $R^2$ ) revealed an energy band gap values of 2.94, 2.77 and 2.62 eV for MIM-0, MIM-50 and MIM-100 samples, respectively. A redshift in the value of the energy band gap by 0.17 and 0.32 eV is achieved via insertion of indium sheets. Indium sheets are less effective in lowering the energy band gap of  $\text{MoO}_3$  compared to Li which lowered the bandgap to 1.78 and 1.10 eV<sup>7</sup> when 50 and 100 nm thick layers of Li were inserted between layers of  $\text{MoO}_3$  films. These two metals differ in the ionic radiuses which cause substitutional effect in  $\text{MoO}_3/\text{Li}/\text{MoO}_3$  and interstitial substitution in the  $\text{MoO}_3/\text{In}/\text{MoO}_3$  samples. It is also worth mentioning that the lowest energy band gap of  $\text{In}_2\text{O}_3$  is reported to be indirect type with value of 2.75 eV [18]. This value is very close to that we determined as 2.77 eV for MIM-50 samples. It is also reported that the indirect energy band gap of  $\text{In}_2\text{O}_3$  could be lowered up to 1.1 eV from that of direct as a result of strong mixing of O  $2p$  and In  $4d$  orbitals [19].

In contrast to that observed in oxides which are known to be highly transparent with energy band gap values larger than 3.0 eV, it is noticeable that the energy band gap of  $\text{MoO}_3$  is less than 3.0 eV. The reason beyond this observation is assigned the crystalline nature and atomic coordinates in  $\text{MoO}_3$ . It is reported that the coordination of  $\text{MoO}_3$  comprises three (singly (O1), doubly (O2) and triply (O3)) symmetrically inequivalent oxygen sites. Each distorted Mo octahedron is composed of an Mo atom bound to one O1 atom, two O2 atoms, and three O3 atoms [15]. It is reported that each oxygen vacancy leads to the creation of polaron. The coordination of O1 display the least formation energy compared to O2 and O3. The formation energies of these are 1.85, 2.19, and 3.20 eV, respectively. Thus, the value of the energy band gap being less than 3.0 eV is ascribed to the transitions between Mo and O3 and Mo and O1, respectively.

Fig. 4b (b) display the value of the real part of the dielectric constant ( $\epsilon_r$ ) spectra. The dielectric constant is calculated from Fresnel's equations for normal incidence of light.<sup>20</sup> The dielectric spectra of the two stacked layers of  $\text{MoO}_3$  display three resonance peaks centered at 3.39, 2.74 and 1.74 eV, respectively. Insertion of sheets of indium of thicknesses of 50 nm resulted in the disappearance of the lowest peak (1.75 eV) and redshifts the other two peaks to 3.09 and 2.13 eV, respectively. Raising the thickness of indium sheets to 100 nm shifts the peaks which were observed at 3.09 and at 2.13 eV in MIM-50 samples to 2.95 and 2.00 eV, respectively. Remarkable enhancement in the value of the dielectric constant is also observed via insertion of indium sheets. Particularly, the maximum value of  $\epsilon_r$  being 6.84 which was observed at 2.74 eV, exhibit value of 9.24 at 3.09 eV and value of 16.20 at 2.94 eV when indium sheets of thicknesses of 50 and 100 nm, respectively, are inserted in between two layers of  $\text{MoO}_3$ . This case is opposite to what was achieved via Li insertion between layers of  $\text{MoO}_3$ . Increasing the thickness of Li in  $\text{MoO}_3/\text{Li}/\text{MoO}_3$  remarkably decreased the value of  $\epsilon_r$ .<sup>7</sup> Namely, insertion of 50 nm thick layers of Li decreased the value of  $\epsilon_r$  from 5.7 (observed at 2.54 eV) to 1.89. Thus, the indium sheets appears to be more effective in enhancing the dielectric performance of the molybdenum trioxide films. In the same context, while the resonance peak being at 3.39 eV could be assigned to the binding energy of the Mo-O bonds [21], the value being 2.74 eV is assigned to the indirect electronic transitions from the valence to the conduction band of  $\text{MoO}_3$  [22]. The 2.74 eV value is also regarded as (lowest unoccupied molecular orbital) LUMO band gap in  $\text{MoO}_3$ . In addition, this value of critical energy is closed to that we observed at 2.72 eV for  $\text{MoO}_3$  in which it was assigned to the transitions between the deep levels of  $\text{Mo}^{5+} d_{yz}^2 - d_{xz}^2$  [15]. Owing to the absence of indium from this sample and the appearance of this energy value (2.74 eV) in the dielectric spectra, it is possible to conclude that the lowering in the energy band gap to 2.77 eV may not be due to In-O transitions but due to the strained structure which may force attenuations in the energy bands. The critical energy value which causes resonance at 1.74 eV in the pure  $\text{MoO}_3$  films may be ascribed to the defective structure. The disappearance of this peak upon insertion of indium sheets

make this prediction stronger as the indium significantly lowered the defect density by 85.2% in MIM-100 samples. In addition, the lowering in the critical energy values which are observed in  $\epsilon_r$  spectra upon indium sheets insertion may be ascribed to the exchange in the bonding mechanism.

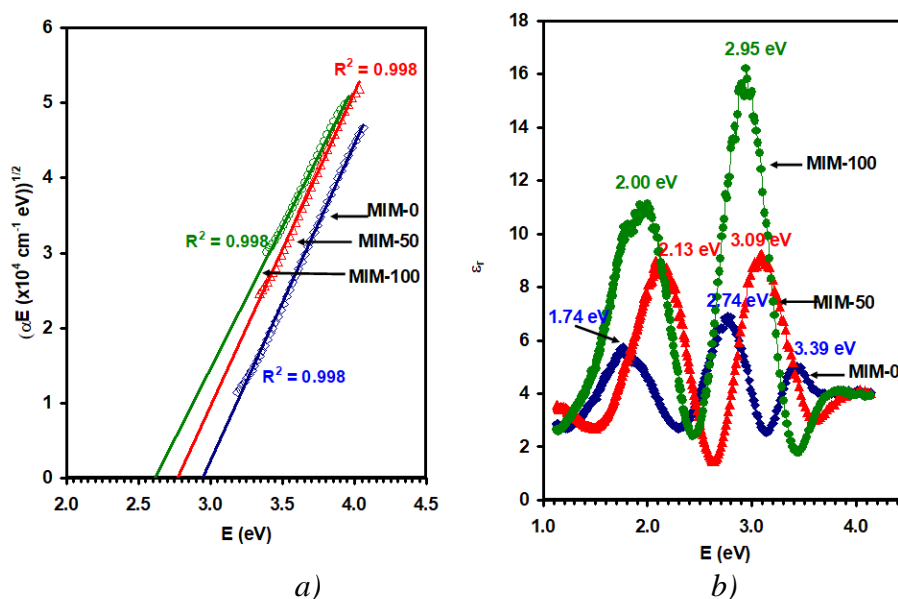


Fig. 4. (a) the  $(\alpha E)^{1/2} - E$  variation and (b) the dielectric constant spectra for the  $\text{MoO}_3/\text{In}/\text{MoO}_3$  films.

Fig. 5 illustrates the optical conductivity spectra ( $\sigma = \frac{\omega \epsilon_{im}}{4\pi}$ ;  $\omega$ : angular frequency) which is calculated from the imaginary part of the dielectric ( $\epsilon_{im}$ ) spectra for the studied samples.  $\epsilon_{im}$  is calculated from the measured transmittance and reflectance data using the previously described techniques [7, 20]. The importance of these parameters lay in the information they provide about the optical conduction parameters like the scattering time at femtosecond level ( $\tau$ ), the electron-plasmon reduced frequency ( $w_e$ ), the drift mobility ( $\mu$ ) and the plasmon frequency ( $w_{pe}$ ). These parameters identify the limits of the wave propagation in the samples and determine the cutoff frequency (plasmon frequency) at which incident electromagnetic waves are transmitted or rejected. As the figure shows, for the MIM-0 samples, the optical conductivity is significant at high incident photon energies only.

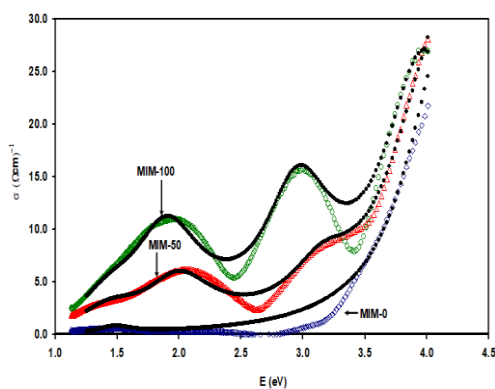


Fig. 5. The optical conductivity spectra the  $\text{MoO}_3/\text{In}/\text{MoO}_3$  films. The dark circles show the fitting of the conductivity with the help of Eqn. (1).

Particularly, the optical conduction starts at energies larger than the energy band gap (2.94 eV). Insertion of indium sheets between the MoO<sub>3</sub> layers enhanced the values of the optical conductivity values and forced responsivity at lower energies. Particularly, the significant optical conduction dominate above 2.70 and above 1.1 eV in the MIM-50 and MIM-100, samples, respectively. Modeling the optical conductivity by the Drude-Lorentz approach was possible using the equations [7, 20],

$$\sigma(\omega) = \sum_{i=1}^k \frac{w_{pi}^2 \omega^2}{4\pi((w_{ei}^2 - \omega^2)^2 + w^2 \tau_i^{-2})}, \quad (1)$$

and

$$w_{pi} = \sqrt{\frac{4\pi n e^2}{m^*}}. \quad (2)$$

In Eqn. 2,  $m^*$  represent the reduced effective masses of MoO<sub>3</sub> or MoO<sub>3</sub>/In/MoO<sub>3</sub> and  $n$  is the free electron density. Substituting  $m_{MoO_3}^* = 0.6m_o$ <sup>7</sup> and ( $m_{In}^* = 1.02m_o$  [23]) to find the reduced effective masses for the MIM-50 and MIM-100 samples through the equation,  $m_{MIM-50 \text{ or } 100}^* = \left(\frac{2}{m_{MoO_3}^*} + \frac{1}{m_{In}^*}\right)^{-1} = 0.229m_o$  and executing the series up to  $k = 5$ , it was possible to reproduce the conductivity spectral data. The curves of the fitting procedure are shown by solid circles in Fig. 5. The results of the fitting procedure are also shown in Table 1.

Table 1. Optical conductivity parameters for the MoO<sub>3</sub>/In/MoO<sub>3</sub> samples.

	MIM-0 n-type					MIM-50 n-type					MIM-100 n-type				
	1	2	3	4	5	1	2	3	4	5	1	2	3	4	5
$\tau_i$ (fs)	2.00	1.50	1.00	0.85	0.85	1.00	1.00	1.00	0.85	0.85	1.00	1.00	1.00	0.85	0.85
$w_e$ ( $\times 10^{15}$ Rad/s)	2.25	5.00	5.50	6.30	7.0	2.20	3.05	4.80	6.00	6.65	2.20	2.90	4.50	6.10	6.00
$n$ ( $\times 10^{17}$ cm <sup>-3</sup> )	7.00	1.00	55	400	600	22.0	45.0	45.0	120	400	30.0	88.0	120	120	170
$\mu$ (cm <sup>2</sup> /Vs)	5.86	4.39	2.93	2.49	2.49	6.39	6.39	6.39	5.43	5.43	6.39	6.39	6.39	5.43	5.43
$w_{pe}$ (GHz)	0.64	0.24	0.24	5.69	5.94	1.68	2.40	2.40	3.92	7.17	1.96	3.36	3.92	3.92	4.67

The table suggests that the effective time at femtosecond level decreases with increasing reduced frequency ( $w_e$ ). In addition, for any of the samples, the higher the reduced frequency the more free electrons available for conduction. For MIM-0 samples, the increase in the free electron density upon increased  $w_e$  leads to sharp decrease in the drift mobility values. It is also noticeable that for the same samples (MIM-0), the plasmon frequency is mostly in the megahertz range indicating the ability of filtering radiowaves only. The insertion of indium sheets remarkably increased the values of the plasmon frequency to gigahertz range and make the MoO<sub>3</sub> samples more appropriate for microwave technology as band filters. For the first oscillator ( $i = 1$ ), the plasmon frequency increased from 0.64 GHz to 1.68 GHz and reached 1.96 GHz as the indium content increased from zero to 3.77 at.% and reaches 12.46 at. %, respectively. The enhancement in the plasmon frequency is accompanied with more stable drift mobility values (the mobility remain constant for the first three oscillators ( $i = 1, 2, 3$ )). It is also noticeable that for the first oscillator ( $i = 1$ ), the indium sheets raised the free electron density from  $7.0 \times 10^{17} \text{ cm}^{-3}$  to  $2.2 \times 10^{18} \text{ cm}^{-3}$  upon insertion of indium sheets of thickness of 50 nm. The free electron density reaches  $3.0 \times 10^{18} \text{ cm}^{-3}$  as indium thickness increased to 100 nm.

On the other hand, comparing the currently tabulated optical conductivity parameters with those we previously reported for lithium sandwiched MoO<sub>3</sub><sup>7</sup> one can see that while the lithium sheets enhanced the drift mobility of MoO<sub>3</sub> better than indium sheets, the indium sheets are more effective in raising the plasmon frequency values. The numerical values suggest that, the plasmon frequency reaches 0.66 GHz for MoO<sub>3</sub>/Li(100 nm)/MoO<sub>3</sub> and 1.68 GHz for MIM-100 samples. It

is also observed that while indium sheets are more effective in changing the crystal structure of  $\text{MoO}_3$  through inducing the crystallization process, it was not able to alter the structure of  $\text{Ga}_2\text{S}_3$  but succeed in engineering the energy band gap of  $\text{Ga}_2\text{S}_3$  in wider range of energy [23]. Even though the structure remained amorphous, the optical conductivity parameters is improved significantly.

It is also worth reminding that our earlier investigations<sup>8</sup> about the same samples (MIM) which are coated onto Au substrates and electrically analyzed predicted the wave filtering features for frequencies near 1.60 GHz. The Au/MIM/C samples exhibited negative capacitance (NC) effects above 1.1 GHz. The spectral studies of impedance indicated the presence of low pass and high pass filters characteristics in the low and high frequency domains, respectively. The AU/MIM/C samples which are found to be suitable for applications as microwave cavities and parasitic capacitance cancellers in electronic circuits are highly consistent with the currently reported information. Table-1 provides information about the plasmon frequencies. The plasmon frequency determines the values where the MIM device will behave as band pass, band stop and band reject filters [24, 25]. The suggested values of limiting frequencies are consistent with the previously published ones confirming the good correlation between the Drude-Lorentz prediction and the experimentally verified results [8, 24]. On the other hand, the currently reported features of band pass filters are combatable with other differently designed materials like  $\text{BaTiO}_3@\text{C-500}$  composites [26, 27]. The later displayed effective bandwidth of  $\sim 5.9$  GHz with minimum return loss value -30.1 dB. The comparison of the dielectric constant values with those of  $\text{Mn}_{1-2x}\text{Zr}_x\text{Fe}_{2-y}\text{Co}_y\text{O}_4$  ( $x=0.00, 0.02, 0.04, 0.06, 0.08, 0.10$  and  $y=0.00, 0.06, 0.12, 0.18, 0.24, 0.30$ ) which were synthesized by micro-emulsion technique, the MIM device can be nominated as future high frequency devices [27].

#### 4. Conclusions

In the current study we explored the effect of insertion of indium sheets on the structural, optical and dielectric performance of molybdenum oxide thin film. Raising the thickness of indium sheets from 50 to 100 nm was sufficient to induce the crystallization process in  $\text{MoO}_3$  without heat treatment or any additional physical constraint. The indium sheets lowered the energy band gap, remarkably increased the dielectric constant and enhanced the optical conductivity of the molybdenum oxide films. In addition, the presence of indium as mid-layer between layers of  $\text{MoO}_3$  was able to increase the free carrier density and enhance the plasmon frequency to microwave levels. The improved properties of the  $\text{MoO}_3$  film that are obtained via insertion of indium sheets make the molybdenum trioxide films more appropriate for high- $\kappa$  gate thin film transistor applications and for applications which need high optical conductivity like terahertz band filters.

#### Acknowledgments

This work was carried out the Arab American University-Palestine (AAUP) laboratories with the support of the scientific research council (SRC). For this reason, the authors acknowledge with thanks the SRC of AAUP for the financial and technical support.

#### References

- [1] G. Sun, M. Shahid, Z. Fei, S. Xu, F. D. Eisner, T. D. Anthopolous, M. A. McLachlan, M. Heeney, *Materials Chemistry Frontiers* **3**, 450 (2019).
- [2] Q. LI, R. YAN, Y. Zhang, L. Dong, *Journal of Ovonic Research* **14**, 1 (2018).
- [3] T. Dai, Y. Ren, L. Qian, X. Liu, *J. Electron. Mater.* **47**, 6709 (2018).
- [4] W.-H. Park, G.-N. Lee, J. Kim, *Sensors and Actuators A: Physical* **271**, 251 (2018).

- [5] S. E. Al Garni, A. F. Qasrawi, *Current Applied Physics* **19**, 639 (2019).
- [6] S. Fujii, Y. Hara, *Materials Express* **8**, 189 (2018).
- [7] S. E. Al Garni, A. F. Qasrawi, *Physica E: Low-dimensional Systems and Nanostructures* **114**, 113569 (2019).
- [8] H. K. Khanfar, A. Qasrawi, M. Daraghmeh, M. Abusaa, *Microwave and Optical Technology Letters* **61**, 2866 (2019).
- [9] F. Liu, D. Xue, *Science China Technological Sciences* **58**, 1841 (2015).
- [10] C. L. Medrano-Pesqueira, F. Brown, D. Möncke, D. de Ligny, J. Tanori, T. del Castillo-Castro, *SN Applied Sciences* **1**, 502 (2019).
- [11] X. Wen, Q. Zhang, Z. Shao, *Crystals* **9**, 2019.
- [12] H. Wipf, K. Neumaier, A. Magerl, A. Heidemann, W. Stirling, *Journal of the Less Common Metals* **101** 317 (1984).
- [13] G. Radnoczi, A. Robertsson, H. Hentzell, S. Gong, M. A. Hasan, *J. Appl. Phys.* **69**, 6394 (1991).
- [14] S. R. Alharbi, A. F. Qasrawi, *Physica Status Solidi A* **216**, 1800977 (2019).
- [15] S. E. Al Garni, A. F. Qasrawi, *Physica E: Low-dimensional Systems and Nanostructures* **105**, 162 (2019).
- [16] H. Sinaim, A. Phuruangrat, S. Thongtem, T. Thongtem, *Mater. Chem. Phys.* **132**, 358 (2012).
- [17] M. M. El Oker, E. A. Abou-Saif, S. A. El Sahhar, A. A. Mohamed, *Physica Status Solidi A* **73**, 389 (1982).
- [18] M. Feneberg, J. Nixdorf, C. Lidig, R. Goldhahn, Z. Galazka, O. Bierwagen, J. S. Speck, *Physical Review B* **93** 045203 (2016).
- [19] P. Erhart, A. Klein, R. G. Egdell, K. Albe, *Physical Review B* **75**, 153205 (2007).
- [20] M. Dresselhaus, M. Dresselhaus, *Optical properties of solids Proceedings of the International School of Physics*, 1966.
- [21] M. Chen, U. Waghmare, C. Friend, E. Kaxiras, *The Journal of chemical physics* **109**, 6854 (1998).
- [22] J. Hofer, S. Bengio, G. Rozas, P. Pérez, M. Sirena, S. Suárez, N. Haberkorn, 2019 Electrical conductivity in extremely disordered molybdenum oxynitrides thin films arXiv preprint arXiv:1905.11909
- [23] E. O. Nazzal, A. F. Qasrawi, S. R. Alharbi, *Plasmonics* **13**, 1049 (2018).
- [24] S. E. Al Garni, A. F. Qasrawi, S. R. Alharbi, *Digest Journal of Nanomaterials and Biostructures* **15**, 367 (2020).
- [25] S. R. Alharbi, A. F. Qasrawi, N. M. Khusayfan, *Digest Journal of Nanomaterials and Biostructures* **15**, 471 (2020).
- [26] Z. Y. He, J. F. Zhang, G. Z. Wang, S. H. Shi, and G. P. Wan. *Digest Journal of Nanomaterials & Biostructures* **14**, 547 (2019).
- [27] A. Faisal, M. Akhtar, M. A. Khan, and A. Wadood, *digest journal of nanomaterials and biostructures* **13**, 475 (2018).